

Shot-noise of quantum chaotic systems in the classical limit

Robert S. Whitney

Institut Laue-Langevin, 6, rue Jules Horowitz, BP 156, 38042 Grenoble Cedex 9. France.

24 April 2007 (updated 5 Oct. 2007 & erratum added for Eq. (16) in Dec. 2020)

ABSTRACT

Semiclassical methods can now explain many mesoscopic effects (shot-noise, conductance fluctuations, etc) in clean chaotic systems, such as chaotic quantum dots. In the deep classical limit (wavelength much less than system size) the Ehrenfest time (the time for a wavepacket to spread to a classical size) plays a crucial role, and random matrix theory (RMT) *ceases to apply* to the transport properties of open chaotic systems.

Here we summarize some of our recent results for shot-noise (intrinsically quantum noise in the current through the system) in this deep classical limit. For systems with perfect coupling to the leads, we use a phase-space basis on the leads to show that the transmission eigenvalues are all 0 or 1 — so transmission is noiseless [Whitney-Jacquod, Phys. Rev. Lett. **94**, 116801 (2005), Jacquod-Whitney, Phys. Rev. B **73**, 195115 (2006)]. For systems with tunnel-barriers on the leads we use trajectory-based semiclassics to extract universal (but non-RMT) shot-noise results for the classical regime [Whitney, Phys. Rev. B **75**, 235404 (2007)].

Keywords: Quantum chaos, semiclassics, shot noise, Fano factor, Ehrenfest time, random matrix theory.

1. INTRODUCTION

In recent years it has been possible to make quantum dots clean enough that the electrons have a mean free path significantly longer than the size of the potential that confines them.^{1,2} The electrons move ballistically in such a dot, in a manner strongly related to the *classical* dynamics associated with the dot's confining potential. It has long been observed that when this classical motion is *chaotic*, the properties of a closed quantum dot (such as energy-level statistics close to the Fermi surface) are well-captured by random matrix theory (RMT).^{3,4} However for open quantum systems it has become increasingly clear that the situation is very different, see Fig. 1. The cross-over to non-RMT behaviour happens when an *Ehrenfest time* becomes of order (or greater than) the dwell time (the typical time the particles spend in the chaotic dot).^{5,6} The Ehrenfest times are the times for a wavepacket to spread (under the classical dynamics) from a size of order a wavelength to a classical scale (i.e. system size, lead widths, etc).

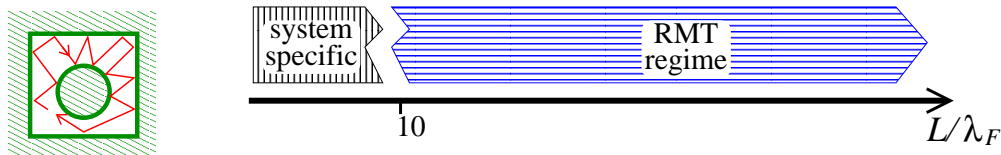
In this article we give a brief overview of our recent results on the nature of quantum noise in the new “classical” regime, where Ehrenfest times are much greater than the dwell time. For more detailed information on the calculations, we refer the reader to the works cited in each section. Similarly those works contain results and discussions on the cross-over from the random matrix regime to the classical regime, which we omit here.

1.1 Quantum dots: a laboratory for quantum chaos

One of the most fundamental questions in quantum mechanics is how the every-day world that we experience emerges from a sea of particles obeying quantum mechanics. Since it is well known that many things in the everyday world are chaotic (the weather, etc), we should try to understand how classical chaos emerges from quantum mechanics.⁷ There are two things one can do to take the classical limit of a quantum system.

- **Vanishing wavelength:** Taking the ratio of the particle's wavelength to all other lengthscales to zero. Usually this means the wavelength becomes much less than the detector size, making quantum interference effects hard to observe.
- **Decoherence:** The particles being studied often interact with other particles in their environment. This can lead to the loss of phase information and the suppression of quantum interference effects.

(a) Closed chaotic systems (level–statistics, etc)



(b) Open chaotic systems (conductance, current noise, conductance fluctuations, etc)

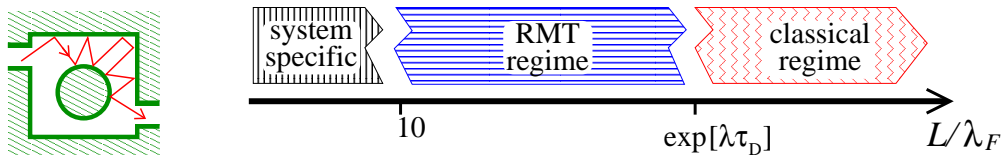


Figure 1. Regimes for closed and open chaotic systems as one goes to the classical limit, when the ratio of system size, L , to wavelength, λ_F , goes to infinity. On the left we have cartoons of classical motion in a chaotic system (Sinai billiard) which is (a) closed and (b) open. Note that we assume that the shape of the system is unchanged as we take $L/\lambda_F \rightarrow \infty$, thus we assume the ratio of lead width, W , to system size remains constant. For an open system the cross-over between the *RMT* and *classical* regimes happens when the Ehrenfest time $\tau_E^{\text{cl}} = \lambda^{-1} \ln[L/\lambda_F]$ grows to become larger than the dwell time, τ_D .

To get experimental insight into quantum chaos, one must take a system whose shape would induce chaos in classical particles, and insert a quantum particle whose wavelength is much smaller than the system size, but *not* immeasurably smaller. Micron-sized (i.e. big) quantum dots are ideal for this, where the wavelength is given by the Fermi surface and is typically a few nanometres. It is crucial that the dots are extremely clean, since impurities typically have a size of order the electron wavelength, and so cause highly quantum (s-wave) scattering, independent of the ratio of L to λ_F . By varying the dot’s temperature, one can control the amount of decoherence.¹³ Thus quantum dots are ideal laboratories for answering the basic questions of quantum chaos. The first experimental observation of the cross-over between the *RMT* and *classical* regimes (Fig. 1b) was made for the a measure of the ratio of shot-noise to current (the Fano factor) in such a device.¹⁴

In different situations, the relative importance of the two classical limits given above (vanishing wavelength and decoherence) are different. Decoherence plays a crucial role in weak-localization^{5, 8, 9} and conductance fluctuations¹⁰ in quantum chaotic dots. However shot-noise is insensitive to decoherence,^{9, 11, 12} so in this article we can neglect decoherence effects entirely.

1.2 Ehrenfest times

Ehrenfest times are the time-scales on which quantum effects start to become relevant in the evolution of a wavepacket. They have acquired this name because Ehrenfest’s theorem (that quantum wavepackets evolve in the same way as a classical probability distributions) is only valid up to these timescales.

We consider a chaotic cavity of size L and Lyapunov exponent λ which is connected to leads of width W ; where L, W are all much larger than the Fermi wavelength, $\lambda_F = \hbar/p_F$. There are Ehrenfest times associated with each classical scale;^{15, 16}

$$\tau_E^{\text{cl}} = \lambda^{-1} \ln [L/\lambda_F] \quad \text{and} \quad \tau_E^{\text{op}} = \lambda^{-1} \ln [(L/\lambda_F) \times (W/L)^2]. \quad (1)$$

The former we call the *closed cavity* Ehrenfest time as it is the only such timescale for a closed chaotic system. The latter we call the *open cavity* Ehrenfest time as it is associated with the presence of leads (although both τ_E^{op} and τ_E^{cl} are relevant in open systems). These scales can be derived as follows. We assume the cavity is a two-dimensional hyperbolic chaotic system. Then the Poincaré surface of section perpendicular to any trajectory is a two-dimensional phase space (r_\perp, p_\perp) , which we make dimensionless by writing distances in units of L and momenta in units of p_F . Then the Liouvillian flow on the Poincaré surface of section stretches exponentially, with

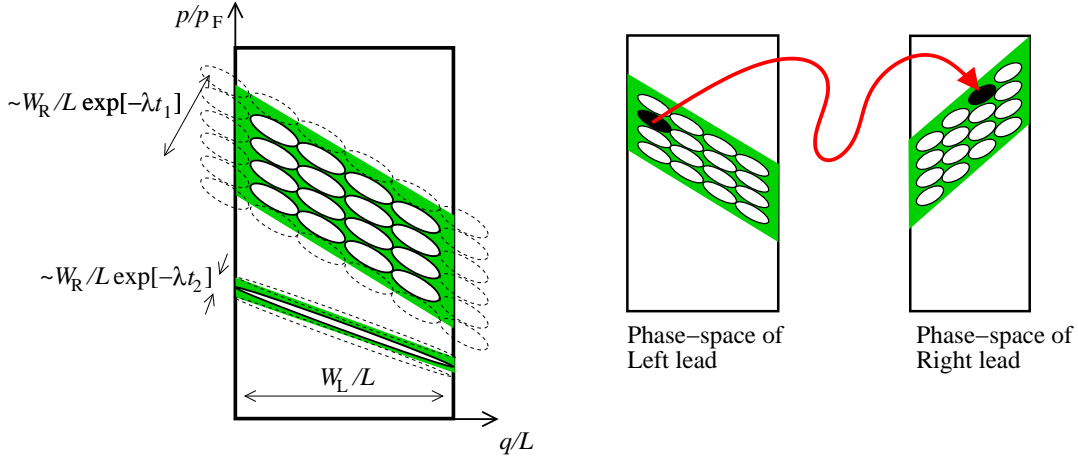


Figure 2. On the left we sketch two bands (in green) on the phase-space of the Left lead. PS-states (ellipses) are super-imposed on these bands. The phase-space is dimensionless, with all lengths and momenta in units of L and p_F , so each ellipse has an area of $\hbar_{\text{eff}} = h/(p_FL)$. The lattice of PS-states has been stretched/rotated to maximize the number of PS-states in each band (solid-edged ellipses) while minimizing the number partially in each band (dashed-edged ellipses). Thus the PS-states have the same aspect ratio as the band. On the right we show the one-to-one correspondence between incoming modes in the band on the Left lead, and outgoing modes in the bands on the Right lead.

rate λ in the *unstable* direction, while contracting exponentially in the *stable* direction. The Ehrenfest times are then given by $\lambda^{-1} \ln[\hbar_{\text{eff}}^{-1} X^2]$ where X is a dimensionless system lengthscale, W/L or 1, and $\hbar_{\text{eff}} = \lambda_F/L$. This is the time for a wavepacket with width X in the *stable* direction (and hence \hbar_{eff}/X in the *unstable* direction) to spread under the Liouvillian flow to width X in the *unstable* direction.

1.3 Shot-noise and transmission eigenvalues

In this article we discuss the zero-frequency shot-noise power, S , for a quantum chaotic systems. This is the intrinsically quantum part of the fluctuations of a non-equilibrium electronic current and it contains information that cannot be obtained through conductance measurements. We give our results in terms of the Fano factor $F = S/S_p$, which is the ratio of S to the Poissonian noise, $S_p = 2e\langle I \rangle$, that a current flow of uncorrelated particles would generate. As such, the Fano factor is a measure of the ratio of the noise to the average current. The scattering theory of transport¹⁷ gives

$$F = \frac{\text{Tr}[\mathbb{S}_{mm_0}^\dagger \mathbb{S}_{mm_0}] - \text{Tr}[\mathbb{S}_{mm_0}^\dagger \mathbb{S}_{mm_0} \mathbb{S}_{mm_0}^\dagger \mathbb{S}_{mm_0}]}{\text{Tr}[\mathbb{S}_{mm_0}^\dagger \mathbb{S}_{mm_0}]}, \quad (2)$$

where \mathbb{S}_{mm_0} is a matrix made up of those elements of the scattering matrix, \mathbb{S} , which correspond to scattering from an ingoing mode on lead m_0 to an outgoing mode on lead m . If we can diagonalize \mathbb{S}_{mm_0} , then it is trivial to extract the Fano factor, since it is given by the following function of the eigenvalues, $\{t_i\}$, of \mathbb{S}_{mm_0} ;

$$F = \frac{\sum_i t_i^* t_i (1 - t_i^* t_i)}{\sum_i t_i^* t_i}. \quad (3)$$

Crucially this means that all modes with an eigenvalue, t_i , which has a magnitude equal to 0 or 1, will *not* contribute to the noise.

2. PS-BASIS: DIAGONALIZING MOST OF THE SCATTERING MATRIX^{18,19}

2.1 Bands in the classical phase-space

The finiteness of τ_D (the dwell time for trajectories in the cavity) means that classical trajectories injected into a cavity are naturally grouped into transmission and reflection bands^{20,21} in phase-space (PS), despite the

ergodicity of the associated closed cavity. Each band on the PS cross-section of the L lead (see Fig. 2) consists of a group of classical paths which exit through the same lead after the same number of bounces, τ , (having followed similar paths through the cavity). Because of the chaotic classical dynamics, bands with longer escape times are narrower, having a width (and hence a PS area) scaling like $\propto \exp[-\lambda\tau]$. The open-cavity Ehrenfest time, τ_E^{op} , is the time at which this area becomes smaller than \hbar . Thus for times *shorter* than this, $\tau < \tau_E^{\text{op}}$, a band can carry one (or more) *orthogonal* quantum wavepackets. We argue below that these can be associated with PS-states (lead modes in the phase-space basis) which behave *classically*. Hence the number of transmitting *classical* PS-states is given by the area of the L lead's phase-space which couples to transmitting trajectories with $\tau < \tau_E^{\text{op}}$. The total number of classical modes in the L lead is the sum of this and the bands which reflect in a time $\tau < \tau_E^{\text{op}}$;

$$N_L^{\text{cl}} = N_L(1 - e^{-\tau_E^{\text{op}}/\tau_D}) \quad (4)$$

where we assume the leads have similar enough width that the Ehrenfest time for transmission and reflection are almost the same.¹⁹ All other modes of the L lead sit over many transmission or reflection bands with $\tau > \tau_E^{\text{op}}$, and so they are *quantum* PS-states; thus $N_L^{\text{qm}} = N_L e^{-\tau_E^{\text{op}}/\tau_D}$. We can do the same for the phase-space of the R lead by replacing L with R throughout.

2.2 Scattering matrix in the phase-space basis

We now summarize the construction of the PS-basis; a basis made of states that are all localised in phase-space (for details see Ref.¹⁹). We cover all phase-space bands with areas bigger than $2\pi\hbar$ with a lattice of PS-states of the form shown in Fig. 2. The lattice is stretched and rotated to optimally cover each band. We can use wavelet analysis to ensure that the lattice of states covering each such band is *complete* and *orthonormal* (within each band). We choose the lattice's position on each band such that each ingoing PS-state evolves under the cavity dynamics to exit as exactly one outgoing PS-state. In this construction, each basis states exits at a time less than τ_E^{op} . It behaves completely *deterministically*, i.e. like a classical particle. It exits as a single wavepacket at a single time through a single lead, completely hiding its quantum nature.

We complete the basis by covering the remaining phase-space (covered in classical bands with phase-space area less than $2\pi\hbar$) in whatever manner is required to complete the orthonormal basis. The basis is already complete on the bands with area larger than $2\pi\hbar$, so each remaining PS-states must sit on many bands in the classical phase-space which exit at many different times through different leads. Thus these PS-basis states exhibit strongly quantum behaviour, however for $\tau_E^{\text{op}} \gg \tau_D$ the proportion of such quantum states vanishes.

The basis of lead modes and the PS-basis are related to each other by a *unitary* transformation, because both bases are complete and orthonormal. Such a transformation leaves the eigenvalues of the scattering matrix, \mathbb{S} , unchanged. As such the transformation should not change any of the transport properties of the system (they all involve only traces of products of $\mathbb{S}_{mm_0}^\dagger \mathbb{S}_{mm_0}$). The scattering matrix in the PS-basis is,

$$\mathbb{S} = \mathbb{S}_{\text{cl}} \oplus \mathbb{S}_{\text{qm}} = \begin{pmatrix} \mathbb{S}_{\text{cl}} & 0 \\ 0 & \mathbb{S}_{\text{qm}} \end{pmatrix} \quad (5)$$

The one-to-one correspondence between ingoing and out-going modes on each band means that \mathbb{S}_{cl} has only one non-zero element in each row and column. If for a system with two leads (L and R), we re-order the labels of the modes on L and R, we can write^{18,19}

$$\mathbb{S}_{\text{cl}} \equiv \begin{pmatrix} \mathbf{r}_{\text{cl}} & \mathbf{t}'_{\text{cl}} \\ \mathbf{t}_{\text{cl}} & \mathbf{r}'_{\text{cl}} \end{pmatrix} \quad \text{with} \quad \mathbf{t}_{\text{cl}} = \begin{pmatrix} \tilde{\mathbf{t}}_{\text{cl}} & 0 \\ 0 & 0 \end{pmatrix} \quad \text{and} \quad \mathbf{r}_{\text{cl}} = \begin{pmatrix} 0 & 0 \\ 0 & \tilde{\mathbf{r}}_{\text{cl}} \end{pmatrix}. \quad (6)$$

The matrices $\tilde{\mathbf{t}}_{\text{cl}}$ and $\tilde{\mathbf{r}}'_{\text{cl}}$ are $n \times n$, where $n = [N_L N_R / (N_L + N_R)] \exp[-\tau_E^{\text{op}}/\tau_D]$ is the number of *classical transmission modes*. The matrix $\tilde{\mathbf{r}}_{\text{cl}}$ is $(N_L^{\text{cl}} - n) \times (N_L^{\text{cl}} - n)$ and $\tilde{\mathbf{r}}'_{\text{cl}}$ is $(N_R^{\text{cl}} - n) \times (N_R^{\text{cl}} - n)$. The matrix $\tilde{\mathbf{t}}_{\text{cl}}$ is diagonal with elements given by $\tilde{t}_{ij} = e^{i\Phi_i} \delta_{ij}$. The matrix $\tilde{\mathbf{r}}_{\text{cl}}$ has a slightly more complicated structure, but it still has exactly one non-zero element in each row and each column. Thus we have diagonalized N_L^{cl} of the modes of \mathbb{S} . It has n modes with eigenvalues obeying $|t_i| = 1$ and $N_L^{\text{cl}} - n$ modes with eigenvalue $t_i = 0$. From Eq. (3),

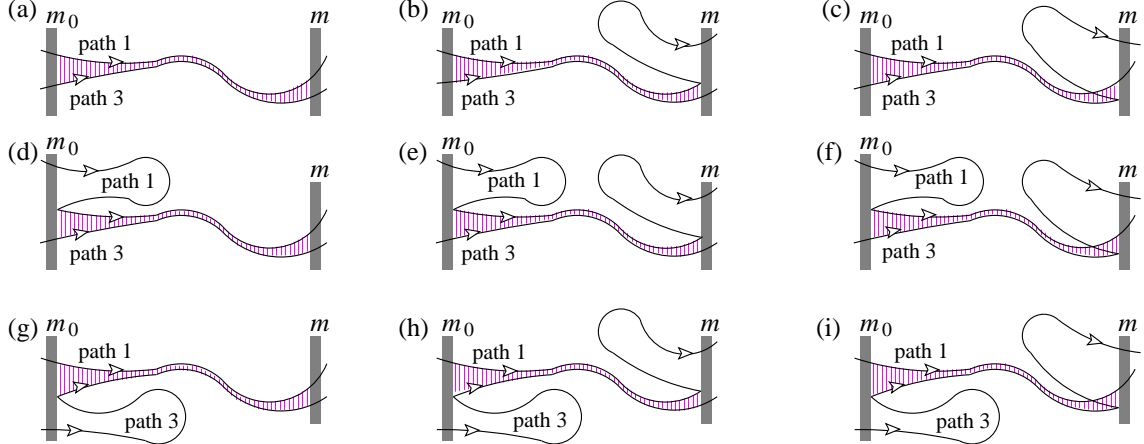


Figure 3. Calculating the shot-noise in the presence of tunnel-barriers. The set of contributions to $\text{tr}[\mathbb{S}_{mm_0}^\dagger \mathbb{S}_{mm_0} \mathbb{S}_{mm_0}^\dagger \mathbb{S}_{mm_0}]$ which do not vanish for infinite Ehrenfest time. Here we show only the tunnel-barriers on leads m_0 and m as shaded rectangles, a path which crosses the barrier on lead m has succeeded in tunnelling out of the cavity into the lead. The contributions are made up of four classical paths, here we show only two of the paths (1 and 3). The other two paths (2 and 4) look the same as the paths shown, *except* that they cross at the centre of the correlated region (indicated by the vertical cross-hatching). Thus path 4 is paired with path 1 at lead m_0 but paired with path 3 at lead m (and vice-versa for path 2). The noise in these contribution is purely due to the stochastic nature of scattering at the tunnel-barriers, if the barriers were absent these contributions would be noiseless.

we see that all these modes are noiseless. In the classical limit the proportion of such classical (noiseless) modes goes to one.²² The remaining modes remain numerous, but their proportion goes to zero. They are quantum in nature and are unitary *within* their own subspace, \mathcal{S}_{qm} .

This gives a microscopic proof of an earlier prediction that the transmission eigenvalues behave as if the system splits into two systems in parallel (one classical, one quantum);²¹ however it does not say anything about whether the quantum system has RMT behaviour or not. As the classical modes are *noiseless*, all noise is generated by the quantum modes. Thus we can expect the Fano factor \propto (2nd moment of noise/average current) to scale like $\exp[-\tau_E^{\text{op}}/\tau_D]$, vanishing as $\hbar \rightarrow 0$. This fits numerical and experimental¹⁴ observations and has agreement with the earlier microscopic theory.⁶

After performing this phase-space analysis, we were able to apply a more traditional (real-space) semiclassical approach to the Fano factor²³ (thereby reproducing Ref.⁶), this was then extended to the third-moment of the noise.²⁴ These works show that the quantum modes do indeed fit RMT (for the reduced part of the scattering matrix that they inhabit) up to at least the third moment of the noise. However we caution the reader that this *effective-RMT conjecture*²¹ does not work for other quantities, such as weak-localization.²⁵

3. SHOT-NOISE WITH TUNNEL-BARRIERS²⁶

We now consider a situation where the leads are not perfectly coupled to the chaotic system. Instead the particles must tunnel through a barrier to enter or leave the system. We consider the limit where the ratio of L, W to λ_F goes to infinity while the tunnelling probability, ρ , remains constant. This is *not* the standard classical limit, because it requires that the thickness of the barriers scale with λ_F not L . However if this thickness were to scale with L , then all barriers would become impenetrable in the classical limit, and there would be no interesting physics to investigate! With tunnel-barriers, the phase-space splitting method no longer works; the barriers mix the PS-basis states because the wavepacket is part transmitted and part reflected each time the wavepacket hits a barrier. Thus instead we added tunnelling effects to the trajectory-based semiclassical method²⁶ previously used for noise without barriers^{23,27} (see also work on quantum graphs²⁸).

In the deep classical limit, $\tau_E^{\text{op}} \rightarrow \infty$, all contributions (to lowest order in $1/N$) are listed in Fig. 3. The contributions involve classical paths (path 1 and 3) which are paired (closer than W with almost parallel momenta)

in the cross-hatched region. The encounter is at the centre of this cross-hatched region, it is shown in detail in Fig. 4. The distance between the paths at the encounter is of order $(\lambda_F L)^{1/2}$, the reason for this will be sketched below. The paths then diverge from each other as they move away from the encounter. However in the deep classical limit the time, $\tau_E^{\text{op}}/2$, for paths to spread from a distance apart $(\lambda_F L)^{1/2}$ to a classical scale become much larger than the dwell time. Thus one or both paths will escape *before* their flow under the cavity dynamics makes them become unpaired (diverge to a distance apart greater than W).

The denominator and the first term in the numerator of Eq. (2) are equal to the dimensionless Drude conductance from lead m_0 to lead m , $g_{mm_0}^{\text{D}} = \rho_{m_0} \rho_m N_{m_0} N_m / (\sum_{m'} \rho_{m'} N_{m'})$. To get this result one simply notes that there are N_{m_0} incoming mode, each of which has a probability of ρ_{m_0} to tunnel into the chaotic system, and then a probability of $\rho_m N_m / \sum_{m'} \rho_{m'} N_{m'}$ of eventually escaping into the m th lead. However to find the Fano factor we must also evaluate $\text{Tr}[\mathbb{S}_{mm_0}^\dagger \mathbb{S}_{mm_0} \mathbb{S}_{mm_0}^\dagger \mathbb{S}_{mm_0}]$. We can write this as the following sum over four paths,

$$\text{Tr}[\mathbb{S}_{mm_0}^\dagger \mathbb{S}_{mm_0} \mathbb{S}_{mm_0}^\dagger \mathbb{S}_{mm_0}] = \frac{1}{(2\pi\hbar)^2} \int_L dy_{01} dy_{03} \int_R dy_1 dy_3 \sum_{\gamma_1, \dots, \gamma_4} A_{\gamma_4}^* A_{\gamma_3} A_{\gamma_2}^* A_{\gamma_1} \exp[i\delta S/\hbar], \quad (7)$$

$$\text{where } \gamma_1 \text{ goes from } y_{01} \text{ to } y_1, \quad \gamma_2 \text{ goes from } y_{03} \text{ to } y_1, \quad \gamma_3 \text{ goes from } y_{03} \text{ to } y_3, \quad \gamma_4 \text{ goes from } y_{01} \text{ to } y_3, \quad (8)$$

with y_{01}, y_{03} on lead m_0 and y_1, y_3 on lead m . The amplitude A_γ is related the square-root of the stability of the path (its exact form is given in Ref.²⁶) and $\delta S = S_{\gamma_1} - S_{\gamma_2} + S_{\gamma_3} - S_{\gamma_4}$ (we have absorbed all Maslov indices into the actions S_{γ_i}). The dominant contributions that survive averaging over energy or cavity shape are those for which the fluctuations of $\delta S/\hbar$ are minimal. Their paths are pairwise identical everywhere except in the vicinity of encounters. Going through an encounter, two of the four paths cross each other, while the other two avoid the crossing. They remain in pairs, though the pairing switches, e.g. from $(\gamma_1; \gamma_4)$ and $(\gamma_2; \gamma_3)$ to $(\gamma_1; \gamma_2)$ and $(\gamma_3; \gamma_4)$. Thus in Fig. 3 we show only paths γ_1 and γ_3 . The action difference δS is then given by the difference between the paths close to the encounter, as in the case without tunnel barriers, the integral over all possible encounters is dominated by those where the paths γ_1 and γ_3 come within $(\lambda_F L)^{1/2}$ of each other.^{29,30} The paths are always close enough to their partner that their stabilities are the same. This stability of a classical path can then be related to the path's probability to go to a given point in phase-space. Hence all contributions can be written in the form

$$D_i = \frac{1}{(2\pi\hbar)^2} \int_L d\mathbf{Y}_{01} d\mathbf{Y}_{03} \int_R d\mathbf{Y}_1 d\mathbf{Y}_3 \int dt_1 dt_3 \langle P(\mathbf{Y}_1, \mathbf{Y}_{01}; t_1) P(\mathbf{Y}_3, \mathbf{Y}_{03}; t_3) \rangle \exp[i\delta S_{D_i}/\hbar], \quad (9)$$

where the subscripts 1, 3 indicate paths 1 and 3 respectively. Here $P(\mathbf{Y}, \mathbf{Y}_0; t)\delta\mathbf{Y}\delta t$ is the probability to go from $\mathbf{Y}_0 = (y_0, p_{y0})$ to within $\delta\mathbf{Y} = \delta y \delta p_y$ of $\mathbf{Y} = (y, p_y)$ in a time within δt of t . For an individual system, this has a δ -function on each classical path, however its average over energy or system shape is a smooth function. Here we have to average over a pair of such probabilities in situations in which the paths start or finish close to each other in phase-space. This has the subtlety that when the paths are close to each other their escape probabilities are highly correlated (if one path hits a lead when the other is within W of it, the probability that the second path hits the lead is close to one). Ref.²⁶ discusses the details of how to evaluate such probabilities.

3.1 Evaluating the contributions.

To evaluate all the contributions in Fig. 3, we note that the paths never become uncorrelated under the classical dynamics; they only escape in an uncorrelated manner if one path tunnels while the other does not. This is because we have taken $\tau_E^{\text{op}} \rightarrow \infty$, so that paths with an encounter take an infinite time to become uncorrelated (if the barriers are absent). In this case the details of the encounter are as given in Fig. 4. Thus the action difference between the paths can be evaluated in a manner equivalent to coherent-backscattering with tunnel-barriers,²⁶ and

$$\delta S_{D_i} = (p_\perp + m\lambda r_\perp) r_\perp. \quad (10)$$

for contributions of the form in Fig. 4a. For contributions of the form in Fig. 4b, the action difference is almost the same (the difference has no effect on the integrals²⁶) so we can use Eq. (10) there as well.

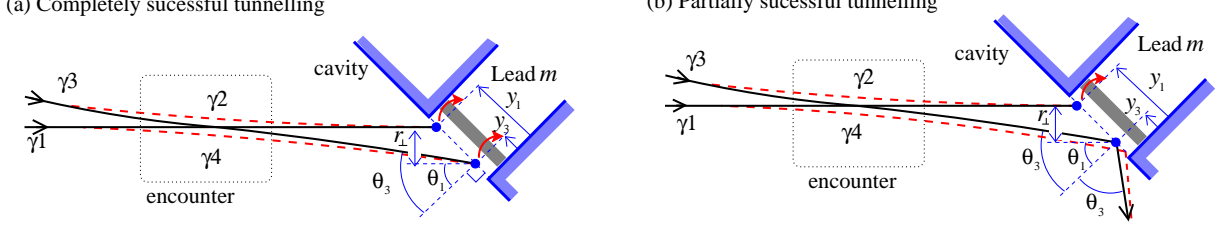


Figure 4. Details of the paths in Fig. 3. Path $\gamma 1$ (solid black line) hits the cross-section of lead m at position y_1 with momentum angle θ_1 , while path $\gamma 3$ hits the lead at (y_3, θ_3) . One path (in this case $\gamma 1$) successfully escapes while the other may (a) succeed in escaping or (b) fail to escape. All paths are drawn in the basis parallel and perpendicular to $\gamma 1$ at escape, the initial position and momentum of path $\gamma 3$ at the lead are $r_{\perp} = (y_1 - y_3) \cos \theta_1$, $r_{\parallel} = (y_1 - y_3) \sin \theta_1$ and $p_{\perp} \simeq -p_F(\theta_3 - \theta_1)$.

For the contribution in Fig. 3a, the paths paired when they hit lead m were also paired at lead m_0 , thus the length of the paired region (cross-hatched in Fig. 3) must be less than T'_W . The time, T'_W , is the time-difference between the paths differing by (r_{\perp}, p_{\perp}) and the *earlier* time when they would have been W apart (if the leads were absent). We find that

$$\int_m d\mathbf{Y}_1 d\mathbf{Y}_3 \int_0^{T'_W} dt_1 dt_3 \langle P(\mathbf{Y}_1, \mathbf{Y}_{01}; t_1) P(\mathbf{Y}_3, \mathbf{Y}_{03}; t_3) \rangle_{1a} = \frac{\rho_m^2 N_m p_F^2 \cos \theta_{01} \cos \theta_{03}}{\sum_{m'} \rho_{m'} (2 - \rho_{m'}) N_{m'}} (1 - \exp[-T'_W / \tau_{D2}]). \quad (11)$$

where τ_{D2} is the survival time for paths which stay extremely close to each other.²⁶ The integral over (r_{\perp}, p_{\perp}) is dominated by $r_{\perp} - (m\lambda)^{-1} p_{\perp} \sim (\lambda_F L)^{1/2}$, as a result the time $T'_W \rightarrow \infty$ in the classical limit, so we can neglect any terms of the form $\exp[-T'_W / \tau_{D2}]$. The denominator comes from the fact we are considering the survival probability for a pair of paths; the probability that the pair is destroyed by one or both paths escaping into a lead during the time t to $t + \delta t$ is $P_2(t) \times \delta t / \tau_{D2}$. We insert Eq. (11) into Eq. (9), then integrate over all possible y_{03} and p_{03} . We find the contribution to $\text{Tr}[\mathbb{S}_{mm_0}^\dagger \mathbb{S}_{mm_0} \mathbb{S}_{mm_0}^\dagger \mathbb{S}_{mm_0}]$ shown in Fig. 3a is

$$D_{1a} = \frac{\rho_{m_0}^2 \rho_m^2 N_{m_0} N_m (1 - \exp[-\tau_E^{\text{op}} / \tau_{D2}])}{\sum_{m'} \rho_{m'} (2 - \rho_{m'}) N_{m'}}. \quad (12)$$

All contribution in Fig. 3 are very similar to D_{1a} . One can see that D_{1b} and D_{1c} are like D_{1a} with the exception that a path is reflected off lead m and then returns to lead m . After reflection that path evolves alone in the cavity. Thus each of these contributions is given by multiplying D_{1a} by

$$\frac{1 - \rho_m}{\rho_m} \times \frac{\rho_m N_m}{\sum_{m'} \rho_{m'} N_{m'}} = \frac{(1 - \rho_m) N_m}{\sum_{m'} \rho_{m'} N_{m'}}, \quad (13)$$

The same applies for paths which enter the cavity from lead m_0 at different times, in such a way that the paths form a pair, as in Fig. 3d (path 3 enters the cavity at a moment when path 1 is reflecting off barrier m_0 , and both paths have similar momenta). To see this we reverse the direction of the paths, after which we have the situation discussed above with m replaced by m_0 . Summing all the contributions in Fig. 3 we get the Fano factor in the deep classical limit ($\tau_E^{\text{op}} \rightarrow \infty$)

$$F = 1 - \frac{\rho_{m_0} \rho_m \sum_{m'} \rho_{m'} N_{m'}}{\sum_{m'} \rho_{m'} (2 - \rho_{m'}) N_{m'}} \left(1 + \frac{2(1 - \rho_{m_0}) N_{m_0}}{\sum_{m'} \rho_{m'} N_{m'}} \right) \left(1 + \frac{2(1 - \rho_m) N_m}{\sum_{m'} \rho_{m'} N_{m'}} \right). \quad (14)$$

If we kept τ_E^{op} finite, the second term would contain a factor of $(1 - \exp[-\tau_E^{\text{op}} / \tau_{D2}])$, however in this case we would not be able to ignore other contributions (given in Ref.²⁶ but neglected above) which go like $\exp[-\tau_E^{\text{op}} / \tau_{D2}]$.

3.2 Shot-noise for a cavity with a third lead

We now consider the special case (shown in Fig. 5) of a cavity with three leads, the current is injected into one and detected at another (neither of which have tunnel barriers), however the current can also go through the

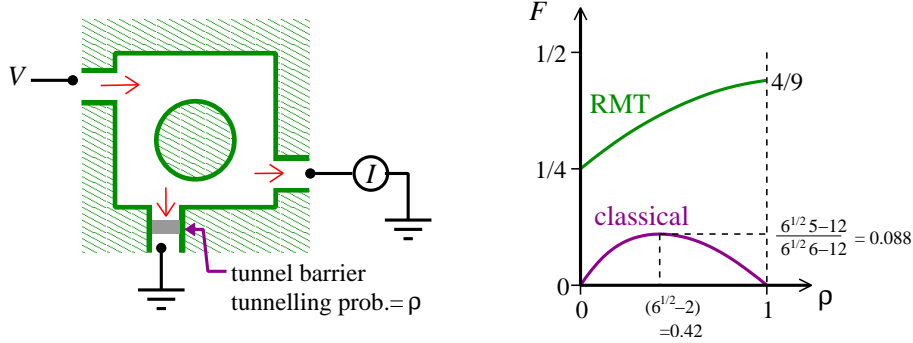


Figure 5. Shot-noise measured in lead 2, when current can also flow into another lead (lead 3). For simplicity we assume all three leads have the same width. On the right we give a cartoon of the Fano factor in the RMT and classical regimes (the exact forms of the functions are given in Eq. (15,16)).

tunnel-barrier into the third lead (where it escapes to earth without being not measured). To keep the formulas as simple as possible we assume all leads have the same width, so each has N modes. Then the Fano factor given in Eq. (14) reduces to

$$F_{3\text{leads}}^{\tau_E^{\text{op}} \rightarrow \infty} = \frac{\rho(1-\rho)}{2+\rho(2-\rho)} \quad (15)$$

where ρ is the transmission probability of the barrier on the third lead. The Fano factor has a maximum at $\rho = \sqrt{6} - 1$, while it is zero (noiseless) when there is no tunnelling, i.e. when the barrier is either impenetrable ($\rho = 0$) or absent ($\rho = 1$). At the maximum the Fano factor is $(5\sqrt{6} - 12)/(6\sqrt{6} - 12)$ (see sketch of curve in Fig. 5). This is completely different from the RMT result for the same system (which is applicable for $\tau_E^{\text{op}} \ll \tau_{D2}$),

$$F_{3\text{leads}}^{\text{RMT}} = \frac{2 + 6\rho + 4\rho^2 + \rho^3}{(2 + \rho)^3}. \quad (16)$$

ERRATUM (16 Dec 2020): Eq. (16)'s numerator should be $2 + 6\rho + 3\rho^2 + \rho^3$.

My thanks to Marcel Novaes for spotting this.

The RMT result goes monotonically from the well-known two-lead result ($F = 1/4$) when $\rho = 0$ to the three-lead result ($F = 4/9$) when $\rho = 1$.

4. CONCLUSION: UNIVERSALITY OF THE CLASSICAL REGIME

We expect that almost any (hyperbolic) chaotic system (Sinai billiard, stadium billiard, kicked-rotator maps, etc) will exhibit the same average properties when coupled to leads. Thus the results presented here for shot-noise in the deep classical limit are *universal* without being given by random matrix theory (RMT). The theory presented here is an ensemble of similar systems (with varying energy or system shape) rather than an individual system. However for shot-noise we can estimate that the typical deviation of an individual system from the average results (calculated above) vanishes in the classical regime (going like the inverse of the number of lead modes).

REFERENCES

1. L.P. Kouwenhoven, C.M. Marcus, P.L. McEuen, S. Tarucha, R.M. Westervelt, and N.S. Wingreen, *Electron Transport in Quantum Dots*, Nato ASI conference proceedings, L.P. Kouwenhoven, G. Schön, and L.L. Sohn (Eds). (Kluwer, Dordrecht, 1997). Y. Alhassid, *Rev. Mod. Phys.* **72**, 895 (2000). I.L. Aleiner, P.W. Brouwer, and L.I. Glazman, *Phys. Rep.* **358**, 309 (2002).
2. C.M. Marcus et al., *Chaos, Solitons and Fractals* **8**, 1261 (1997).
3. O. Bohigas, M. J. Giannoni, and C. Schmit. *Phys. Rev. Lett.* **52**, 1 (1984).

4. S. Heusler, S. Müller, A. Altland, P. Braun, and F. Haake, Phys. Rev. Lett. **98**, 044103 (2007)
5. I.L. Aleiner and A.I. Larkin, Phys. Rev. B **54**, 14423 (1996); Phys. Rev. E **55**, R1243 (1997).
6. O. Agam, I. Aleiner and A. Larkin, Phys. Rev. Lett. **85**, 3153 (2000).
7. F. Haake. *Quantum Signatures of Chaos*. Springer, Berlin (2000).
8. C. Petitjean, Ph. Jacquod and R.S. Whitney, eprint: cond-mat/0612118.
9. R.S. Whitney, Ph. Jacquod and C. Petitjean, in preparation
10. C. Tian, A. Altland, and P.W. Brouwer, Phys. Rev. Lett. **99**, 036804 (2007).
11. C.W.J. Beenakker, Rev. Mod. Phys. **69**, 731 (1997).
12. S.A. van Langen and M. Büttiker, Phys. Rev. B **56**, R1680 (1997)
13. Decoherence effects can be almost neglected at the lowest experimentally-accessible temperatures, but they quickly grow one increases the temperature.
14. S. Oberholzer, E.V. Sukhorukov, and C. Schönenberger, Nature **415**, 765 (2002).
15. M.G. Vavilov and A.I. Larkin, Phys. Rev. B **67**, 115335 (2003).
16. For a review see H. Schomerus and Ph. Jacquod, J. Phys. A. **38**, 10663 (2005).
17. Ya.M. Blanter and M. Büttiker, Phys. Rep. **336**, 1 (2000).
18. R.S. Whitney and Ph. Jacquod, Phys. Rev. Lett. **94**, 116801 (2005).
19. Ph. Jacquod and R.S. Whitney, Phys. Rev. B **73**, 195115 (2006).
20. L. Wirtz, J.-Z. Tang, and J. Burgdörfer, Phys. Rev. B **59**, 2956 (1999).
21. P.G. Silvestrov, M.C. Goorden, and C.W.J. Beenakker, Phys. Rev. B **67**, 241301(R) (2003).
22. We believe Refs.^{18,19} gave the first microscopic proof of this result, despite the fact it was anticipated some time ago; C.W.J. Beenakker and H. van Houten, Phys. Rev. B **43**, R12066 (1991).
23. R.S. Whitney and Ph. Jacquod, Phys. Rev. Lett. **96**, 206804 (2006).
24. P.W. Brouwer, and S. Rahav, Phys. Rev. B **74**, 085313 (2006)
25. S. Rahav and P.W. Brouwer, Phys. Rev. Lett. **95**, 056806 (2005); Phys. Rev. B, **73**, 035324 (2006).
26. R.S. Whitney, Phys. Rev. B **75**, 235404 (2007).
27. P. Braun, S. Heusler, S. Müller, and F. Haake, J. Phys. A: Math. Gen. **39**, L159 (2006). S. Müller, S. Heusler, P. Braun, F. Haake, New J. Phys. **9** 12 (2007).
28. H. Schanz, M. Puhlmann and T. Geisel, Phys. Rev. Lett. **91**, 134101 (2003).
29. M. Sieber and K. Richter, Phys. Scr. **T90**, 128 (2001); M. Sieber, J. Phys. A: Math. Gen. **35**, L613 (2002).
30. K. Richter and M. Sieber, Phys. Rev. Lett. **89**, 206801 (2002).